Journal of
Mechanics of
Materials and Structures

A COCHLEAR MODEL USING THE TIME-AVERAGED LAGRANGIAN AND THE PUSH-PULL MECHANISM IN THE ORGAN OF CORTI

Yongjin Yoon, Sunil Puria and Charles R. Steele

Volume 4, Nº 5 May 2009

mathematical sciences publishers

JOURNAL OF MECHANICS OF MATERIALS AND STRUCTURES
Vol. 4, No. 5, 2009

A COCHLEAR MODEL USING THE TIME-AVERAGED LAGRANGIAN AND THE PUSH-PULL MECHANISM IN THE ORGAN OF CORTI

YONGJIN YOON, SUNIL PURIA AND CHARLES R. STEELE

In our previous work, the basilar membrane velocity V_{BM} for a gerbil cochlea was calculated and compared with physiological measurements. The calculated V_{BM} showed excessive phase excursion and, in the active case, a best-frequency place shift of approximately two fifths of an octave higher. Here we introduce a refined model that uses the time-averaged Lagrangian for the conservative system to resolve the phase excursion issues. To improve the overestimated best-frequency place found in the previous feed-forward active model, we implement in the new model a *push-pull mechanism* from the outer hair cells and phalangeal process. Using this new model, the V_{BM} for the gerbil cochlea was calculated and compared with animal measurements, The results show excellent agreement for mapping the location of the maximum response to frequency, while the agreement for the response at a fixed point as a function of frequency is excellent for the amplitude and good for the phase.

A list of symbols can be found on page 985.

1. Introduction

The cochlea of the inner ear transforms the input sound into output neural excitation. The basic model consists of a long, straight box of fluid with a flat lengthwise partition. The spiral coiling of the cochlea is neglected, as it has been shown to have little effect on the model response [Loh 1983; Steele and Zais 1985]. The partition has an elastic portion called the *basilar membrane* (BM). Generally, this membrane is narrow and thick, and therefore stiff, at the input end, where it connects with stapes, and wide and thin, and consequently flexible, at the far end, the apex. From a sinusoidal pressure input, a traveling fluid-elastic wave is generated on the BM.

For a fixed frequency of input, experiments show a traveling wave on the BM that builds to a peak at a certain point and then rapidly decays as it moves further. The location of the peak depends on frequency; thus each point has a "best frequency" (BF) that causes the maximum amplitude of the BM response. In the actual cochlea, a sensory epithelium, called the organ of Corti, is attached to the BM. The organ of Corti contains the sensory hair cells, which respond to the BM motion and initiate neural excitation. However, three rows of outer hair cells (OHC) are piezoelectric and most likely provide an amplification of the wave for low input amplitude; this is known as the *active mechanism*. Because of the geometry of the outer hair cells, a feed-forward approximation can be used in the cochlear model. Two-dimensional [Geisler and Sang 1995] and three-dimensional models with the active feed-forward mechanism have been employed [Steele et al. 1993; Lim and Steele 2002; Yoon et al. 2007].

Keywords: cochlear active model, basilar membrane velocity, outer hair cell, push-pull mechanism, gerbil.
Work supported by the NIDCD of the National Institutes of Health through grant no. R01-DC007910.

In the present work, we improve on this previous feed-forward active model with further consideration of the actual geometry. For the low amplitude of sound intensity, there is significant energy feedback that enhances the wave. Located on the elastic region is the organ of Corti, which contains the sensory hair cells in an interesting arrangement of structural elements. A possible explanation for the form is derived from an analysis of the effect of the electromotile (piezoelectric) expansion and contraction of the outer hair cells which is known as OHC motility. This motility causes a positive spatial "feed-forward" of force on the basilar membrane (the "push") as well as a negative "feed-backward" of force (the "pull") from the phalangeal process. These push and pull mechanism work together to provide a two order of magnitude increase in the amplitude of the wave for the short wavelengths, but cancel each other out for the long wavelengths. Thus, the significant enhancement occurs in a narrow band of spatial wavelengths, without the need for special filtering or tuning. The calculations for the simple box model of the cochlea with the push-pull mechanism and the "time-averaged Lagrangian" method [Steele and Taber 1979] yield results very similar to gerbil measurements [Ren and Nuttall 2001].

2. Mathematical methods

Passive cochlear model. The physical cochlea is modeled as a straight-tapered fluid-filled chamber with rigid walls. The chamber is divided longitudinally by the flexible orthotropic plate into two equal rectangular ducts, which represent the *scala vestibuli* and *scala tympani*. The two fluid ducts are joined at the apical end of the chamber by a hole, representing the *helicotrema*. The flexible plate represents the pectinate zone of the basilar membrane, which bends under the motion of the fluid driven by the stapes motion. A schematic drawing of the model is shown in Figure 1.

The equations of the system are formulated in the frequency domain. Harmonic excitation is applied at the stapes and the steady-state response of the system is considered. The equation for wave propagation in the passive model is obtained by equating the time-averaged kinetic and potential energies of the conservative system. The detailed derivations and features for the passive mechanics were described in [Steele and Taber 1979]. Briefly, the three-dimensional fluid equations are integrated over the cross section to obtain the relation between volume flow and fluid pressure, using a Fourier series expansion.

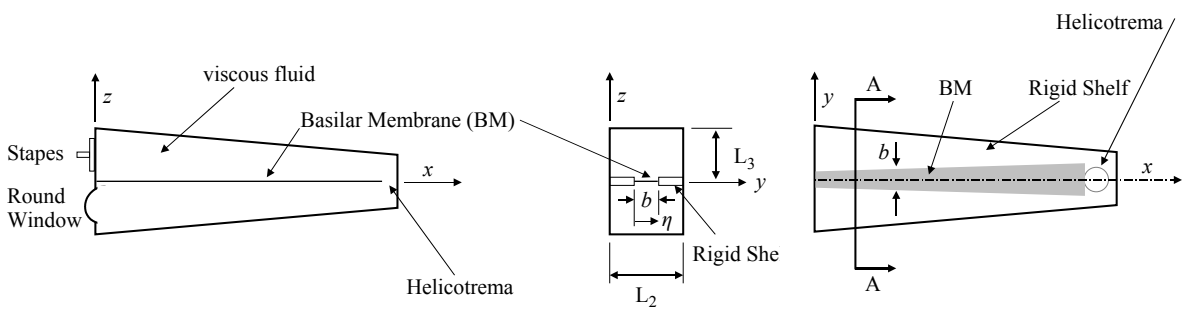

Figure 1. Geometric layout of the passive cochlear model: from left to right, side view, cross section (A-A), and top view. Distances are parameterized in cartesian coordinates, x representing the distance from the stapes, y the distance across the scala width, and z the height above the partition.

The time-averaged kinetic energy of the fluid (T_f) and of the elastic basilar membrane (T_p) are then obtained, as is the time-averaged potential energy of the plate (V_p). By equating the time-averaged kinetic and potential energies of the system, the eikonal equation is obtained, which can be written as

$$L = T_f + T_p - V_p = F(n,\omega)W(x)^2\left(\int_0^b \eta^2(\xi)d\xi\right) = 0. \tag{1}$$

This gives the phase relation for the active case, $F(n,\omega) = 0$, where b is the BM width, n is the wavenumber, and ω is the frequency. Here, L is the time-averaged Lagrangian density of the system, $W(x)$ the amplitude of the wave envelope, and $\eta(\xi) = \sin(\pi\xi/b)$ the shape function for simply-supported edges; the coordinate ξ has its origin at one edge of the BM.

Active cochlear model: push-pull mechanism. For the push-pull active model, the arrangement of the organ of Corti is indicated in Figure 2. If the OHCs expand, the Deiters rod at the horizontal distance $x + \Delta x_1$ will be pushed down by the OHC with the apex at x, and pulled up by the phalangeal process connected to the OHC with the apex at $x + \Delta x_2$. The force in an OHC is proportional to the shear force on the cilia at the apex, which is approximately equal to the total force acting on the BM. This push-pull mechanism is quantified by writing the total force on the BM as

$$F_{\mathrm{PZ}} = 2F^f_{\mathrm{BM}} + F^C_{\mathrm{BM}}. \tag{2}$$

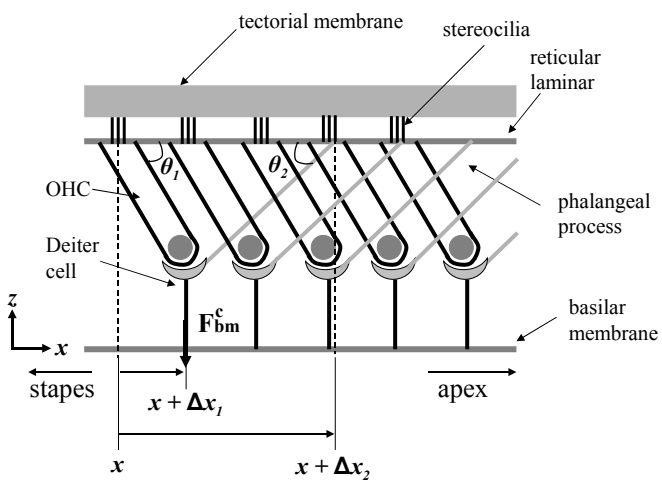

Figure 2. Schematic longitudinal view of the organ of Corti, showing the tilt of the outer hair cells. For one hair cell with apex at the distance x, the base is at $x + \Delta x_1$; the phalangeal process connected at the base attaches to the upper surface at $x + \Delta x_2$; the OHC angle is θ_1; and θ_2 is the angle of the phalangeal process angle with the reticular lamina. The force on the BM through the Deiters rod is $F^c{}_{\mathrm{BM}}$, which consists of the downward push from an expansion of the hair cell at x and an upward pull through the phalangeal process from an expansion of the hair cell at $x + \Delta x_2$.

in which F^C_{BM} is the force due to the OHCs, and F^f_{BM} is the force due to the fluid on one side. The force acting through the Deiters rod at $x + \Delta x_1$ is

$$F^C_{\mathrm{BM}}(x + \Delta x_1) = \alpha_1\big(2F^f_{\mathrm{BM}}(x) + F^C_{\mathrm{BM}}(x)\big) - \alpha_2\big(2F^f_{\mathrm{BM}}(x + \Delta x_2) + F^C_{\mathrm{BM}}(x + \Delta x_2)\big), \tag{3}$$

in which the gains from the push and the pull are α_1 and α_2, respectively, while Δx_1 is the longitudinal distance between the apex and the base of the OHC, which depends on the length l_{OHC} of the OHC and its angle θ_1 with respect to the longitudinal direction to the reticular lamina (see Figure 2):

$$\Delta x_1 = l_{\mathrm{OHC}} \cos\theta_1. \tag{4}$$

Moreover $\Delta x_2 - \Delta x_1$ is the longitudinal distance between the base and the apex of the phalangeal process, which depends on the length l_p of the phalangeal process and its angle θ_2 with respect to the longitudinal direction of the reticular lamina:

$$\Delta x_2 - \Delta x_1 = l_p \cos\theta_2. \tag{5}$$

Based on the geometric relationship between OHC and phalangeal process, l_p can be expressed as

$$l_p = l_{\mathrm{OHC}} \frac{\sin\theta_1}{\sin\theta_2}. \tag{6}$$

By (5) and (6), $\Delta x_2 - \Delta x_1$ can be reduced without l_p:

$$\Delta x_2 - \Delta x_1 = l_{\mathrm{OHC}} \sin\theta_1 \cot\theta_2. \tag{7}$$

From the phase integral, (3) reduces to

$$F^C_{\mathrm{BM}} e^{in\Delta x_1} = \alpha_1(2F^f_{\mathrm{BM}} + F^C_{\mathrm{BM}}) - \alpha_2(2F^f_{\mathrm{BM}} + F^C_{\mathrm{BM}})e^{in\Delta x_2}. \tag{8}$$

The force from the OHC motility is related to the fluid force:

$$F^C_{\mathrm{BM}} = \frac{2(\alpha_1\Gamma_1 - \alpha_2\Gamma_2)F^f_{\mathrm{BM}}}{1 - \alpha_1\Gamma_1 + \alpha_2\Gamma_2}, \tag{9}$$

where

$$\Gamma_1 = e^{-in\Delta x_1} \quad \text{and} \quad \Gamma_2 = e^{in(\Delta x_2 - \Delta x_1)}.$$

Therefore, the total force on the BM from (2) is

$$F_{\mathrm{PZ}} = 2\left(1 + \frac{(\alpha_1\Gamma_1 - \alpha_2\Gamma_2)}{(1 - \alpha_1\Gamma_1 + \alpha_2\Gamma_2)}\right)F^f_{\mathrm{BM}} = \frac{2F^f_{\mathrm{BM}}}{1 - \alpha_1\Gamma_1 + \alpha_2\Gamma_2}. \tag{10}$$

Matching the force to the displacement of the fluid and the OHC to the BM stiffness yields the eikonal (dispersion) relation of the active model. We consider a positive value of α_2 to be a negative feedback effect of the phalangeal processes. Because of the flexibility of the upper surface consisting of the tectorial membrane and the reticular lamina in Figure 2, the upward and downward forces tend to cancel each other, so that $\alpha_1 = \alpha_2$. Then, for the long wavelength, i.e., the small values of the wave number n, the push-pull effect in (2) are negligible, while for very short wavelengths, the fluid viscosity dominates. Thus, the push-pull is effective only in a band of wavelengths. It is assumed that OHC force production does not roll off with frequency and thus α_1 and α_2 are constant with frequency. Although this is controversial,

there is evidence that suggests that OHCs can generate forces for frequencies up to 50 kHz [Rabbitt 2008].

Wave propagation of BM plate. An energy approach is used involving variational calculus which is applied to the time-averaged Lagrangian density L of the system Equation (1). Independent variation of n and $W(x)$ yields the Euler–Lagrange equations

$$\frac{\partial L}{\partial W} = 2F(n,\omega)W(x)\left(\int_0^b \eta^2(\xi)d\xi\right) = 0, \tag{11}$$

$$\frac{d}{dx}\frac{\partial L}{\partial n} = \frac{d}{dx}\left[\frac{\partial F(n,\omega)}{\partial n}W^2(x)\left(\int_0^b \eta^2(\xi)d\xi\right)\right] = 0. \tag{12}$$

The eikonal equation is obtained using (11):

$$F(n,\omega) = 0. \tag{13}$$

The amplitude function, $W(x)$, which is the solution of the transport equation (12), is expressed as

$$W(x) = C\left(\frac{\partial F(n,\omega)}{\partial n}b\right)^{-1/2}, \tag{14}$$

where C is a constant determined from the boundary condition.

Hamilton's principle is valid only for a conservative system; however, nonconservative terms can be added to the Lagrange equations of motion. Thus, we extend Equation (11) and (12) to the push-pull active model to obtain the eikonal and transport equation.

Ratio of the BM velocity to the stapes velocity. For a given harmonic excitation frequency ω, the eikonal equations for the passive and active case are solved to give the wavenumber (n) by using Newton–Raphson iterative scheme for each cross section along the cochlear duct. Once n is determined, the ratio of the BM velocity V_{BM} to the stapes velocity V_{st} is obtained. With the stapes motion defined as positive outward, the ratio at $x = x^*$ is

$$\left(\frac{V_{\mathrm{BM}}}{V_{st}}\right)_{x=x^*} = \frac{2nA_{st}}{b_{x=0}}\left[\frac{\left(b\,\partial F(n,\omega)/\partial n\right)_{x=0}}{\left(b\,\partial F(n,\omega)/\partial n\right)_{x=x^*}}\right]\exp\left(\frac{\pi}{2} - \int n\,dx\right), \tag{15}$$

where A_{st} is the stapes foot-plate area.

Modification for nonconservative system. An extension of the time-averaged Lagrangian method to nonconservative systems is given in [Jimenez and Whitham 1976], in which the adjoint is considered. An alternate approach is to consider the reciprocity principle. For a linear elastic system, consider two independent solutions, denoted by superscript $^{(1)}$ and $^{(2)}$. The stress from (2) multiplied by the displacement of (1) subtracted from the stress from (1) multiplied by the displacement from (2), integrated over the entire surface, must be zero. In standard notation this is

$$\int \boldsymbol{n}\cdot\left(\sigma^{(1)}\cdot\boldsymbol{u}^{(2)} - \sigma^{(2)}\cdot\boldsymbol{u}^{(1)}\right)d\Sigma = 0. \tag{16}$$

This depends on the symmetry of the tensor of elastic constants. The symmetry is preserved when dealing with viscoelastic materials, including a viscous fluid, and working in the frequency domain, for which

the coefficients are complex-valued. For a tube such as the cochlea, in which no work is done on the side walls, the integral over one end is the negative of that over the other end. Since the sign change is due to the change in the direction $\boldsymbol{n}$, the integral itself must be constant with the distance along the tube. So one solution is taken with a positive exponential,

$$\left(\sigma^{(1)}, \boldsymbol{u}^{(1)}\right) \to \exp \int \lambda \, dx, \tag{17}$$

while the other is taken with a negative exponential,

$$\left(\sigma^{(2)}, \boldsymbol{u}^{(2)}\right) \to \exp \int -\lambda \, dx. \tag{18}$$

One is a backward traveling wave, exponentially increasing, while the other is a forward traveling wave, exponentially decreasing. For a conservative system, the condition (16) yields the same result for the transport condition as (14). For a dissipative system with fluid viscosity, we find little difference, since the wave number changes little. In addition, Equation (16) can be used for the case of feedback, when the system is no longer self-adjoint. In this case the second solution in (16) must be taken as a solution of the adjoint problem. Again we find little effect on the solutions for the cochlea, so (14) remains a good approximation.

3. Results and discussion

The cochlear model is used to calculate the response of a gerbil cochlea. The material property values in Table 1 were taken from [Smith 1968; Lim 1980; Steele et al. 1995; Karavitaki 2002], and the dimensions in Table 2 from anatomical measurements for the gerbil cochlea [Sokolich et al. 1976; Greenwood 1990; Dannhof et al. 1991; Cohen et al. 1992; Edge et al. 1998; Thorne et al. 1999; Naidu and Mountain 2007].

The model is meshed into 1200 sections along the 12 mm length of the cochlea. Forty terms are used in the Fourier expansion across the width of the fluid duct. Calculation with eighty terms for the Fourier expansion shows no difference with forty terms. Running on an Intel Pentium IX (3.40 GHz) processor, the average time taken for a single harmonic excitation calculation is about one second. This method provides a fast and efficient solution compared to a full-scale finite element model. Note that the computation time indicated by [Parthasarathi et al. 2000] is measured in hours of computing time for the linear solution for a single frequency.

The results include the BF-to-place map and the BM velocity frequency response. The modeling results for the gerbil cochlea are compared with recent *in vivo* experiment measurements in the cochlea.

scala fluid
$\rho_f = 1.0 \times 10^3$ kg/m^3
$\mu = 0.7 \times 10^{-3}$ Pa s

basilar membrane
$\rho_p = 1.0 \times 10^3$ kg/m^3
$E_{11} = 1.0 \times 10^{-3}$ GPa
$E_{22} = 1.0$ GPa
$E_{12} = 0.0$ GPa
$\nu = 0.5$

outer hair cell
$\theta_1 = 85°$
$\theta_2 = 25°$
$\alpha_1 = 0.14$
$\alpha_2 = 0.14$

Table 1. Gross properties in cochlear model.

x (mm)	b (mm)	h (mm)	f	L_2, L_3 (mm)	l_{OHC} (μm)
0		0.0210	0.030	1.000	25.0
1.5		0.0175		0.707	
2.9	0.162			0.387	
3.5		0.0131			
5.0				0.316	
5.9		0.0088			
7.2	0.190	0.0073		0.282	
8.4					
9.0		0.0055		0.316	
10.2	0.205	0.0044			
12.0		0.0031	0.007	0.245	65.0

Table 2. Property variations in gerbil cochlear model. Notation: b: width of plate; h: plate thickness; h_f: BM fluid thickness; L_2, L_3: width and height of fluid chamber; l_{OHC}: length of outer hair cell length.

CF-to-place map. CF versus distance from the stapes along the gerbil cochlear (CF range: 0.3 kHz–50 kHz) is shown in Figure 3. The gerbil CF-to-place map [Sokolich et al. 1976; Greenwood 1990] was measured with cochlear-microphonic recording. The maps from the passive model and measurement are in excellent agreement (Figure 3).

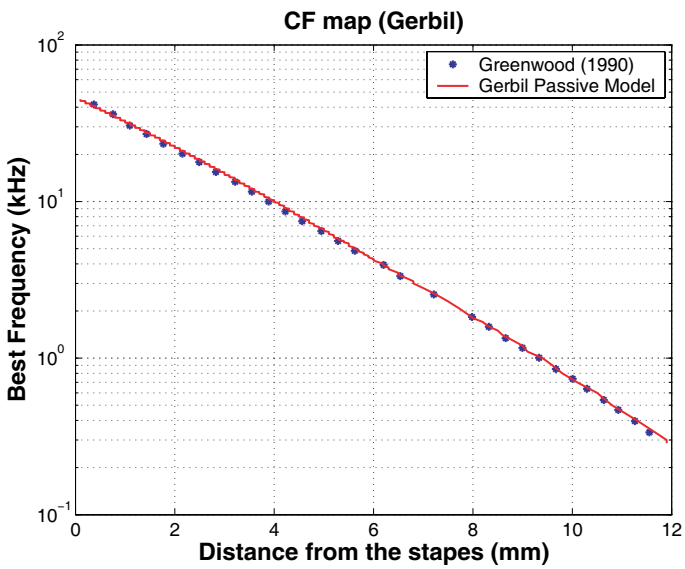

Figure 3. Characteristic frequency (CF) versus position for the passive cochlear model compared to measurements. The present three-dimensional cochlear model represents the gerbil cochlear CF-to-place map from 0.3 kHz to 50 kHz [Sokolich et al. 1976; Greenwood 1990] over a length of 12 mm.

BM velocity frequency response. The gerbil cochlear BM velocity magnitude and phase for 4.2 mm from the base (BF = 10 kHz) relative to the stapes displacement were computed up to 20 kHz and are compared with the gerbil experimental data from [Ren and Nuttall 2001] in Figure 4. The passive model shows quantitatively very good agreement with data which are measured at a high stimulus level (100 dB SPL at the ear canal).

Karavitaki [2002] gives the angle of tilt of gerbil OHC (θ_1) as 84°, closer to perpendicular to the BM (Figure 2). The active model results are calculated with parameters; $\theta_1 = 85°$ (OHC angle), $\theta_2 = 25°$ (phalangeal process angle), $\alpha_1 = \alpha_2 = 0.14$ (feedforward and feedback gain factor). The active model shows qualitatively and quantitatively good agreement with data at low stimulus level (30 dB SPL at the ear canal) with 27 dB gain.

In the left half of Figure 4, showing the magnitude of the relative BM velocity, the calculated BF place shifts from 10 kHz (passive model) to 13 kHz (active model), providing better agreement with measurements. The BF place shift (two fifths of an octave upwards) observed in the earlier feed-forward active model [Yoon et al. 2007] is resolved by using a push-pull mechanism in the active model. From the parameter study, we find that the BF place shifts to the low frequency by using a small phalangeal process angle in the active case.

The right half of Figure 4 shows that we obtain good agreement in the phase as well, at least in the region below the BF place (that is, up to 10 kHz). Reduced phase excursion is one of the most impressive improvements in the time-averaged Lagrangian model, compared to the 2.5 cycle phase difference near BF region in the earlier model. However, past the BF, the phase of BM velocity from the model shows a larger roll-off than the phase from the data, which represents over-fluctuation of the traveling wave after 10 kHz in the model.

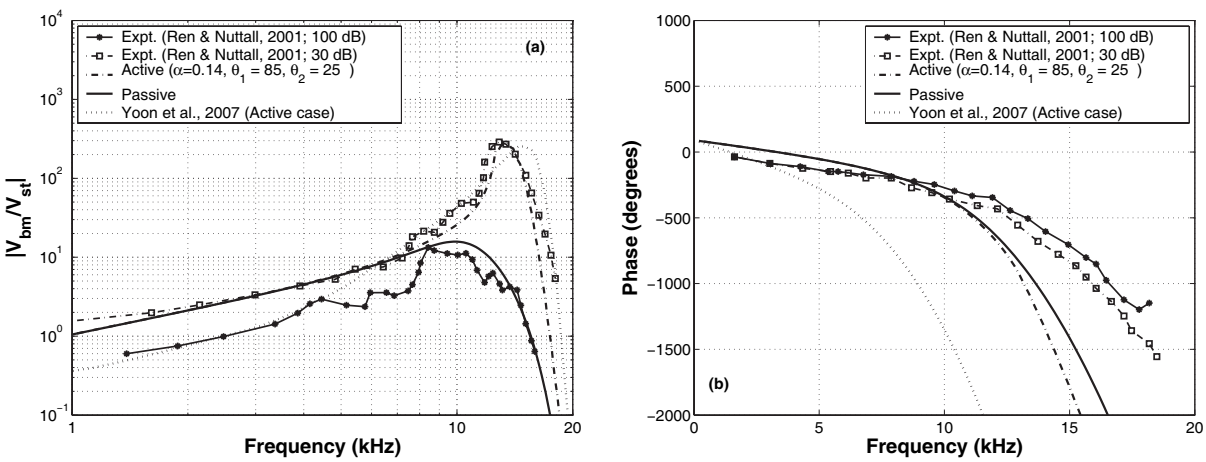

Figure 4. Basilar membrane (BM) velocity relative to the stapes: magnitude (left) and phase (right) for the gerbil cochlea at 4.2 mm from the base (BF = 10 kHz). For the active model, a value of 0.14 was used for the feed-forward and feedback gain factor. Experimental data from [Ren and Nuttall 2001] are included for comparison. Results from our earlier model [Yoon et al. 2007] are presented in dotted lines.

4. Conclusions

We presented a refinement of an earlier physiologically based three-dimensional cochlear model [Yoon et al. 2007] that resolved its two main deficiencies: a relatively large phase excursion near the best frequency region, which was addressed using the time-averaged Lagrangian method, and an overestimation of the best frequency (by about two fifths of an octave) observed in the earlier feed-forward active model, which was ameliorated by the implementation of a push-pull mechanism in the active case. Basilar membrane velocity simulation results for the gerbil cochlea now show excellent agreement in magnitude and good agreement in phase relative to physiological measurements. However, past the best frequency region, the phase in the current model still shows excessive roll-off. We hope that this can be addressed by incorporating into the model a more detailed treatment of the organ of Corti [Steele and Puria 2005].

List of symbols

BM	basilar membrane	L_2, L_3	width and height of fluid chamber
OHC	outer hair cell	α_1, α_2	feed-forward and feedback gain factors
BF	best frequency	l_{OHC}, l_p	length of OHC, length of phalangeal process
n	wave number	θ_1, θ_2	angle of tilt of OHC, phalangeal process
x, y, z	Cartesian coordinates	F_{PZ}, F^f_{BM}	forces acting on the pectinate zone and fluid
ω	angular velocity	F^C_{BM}	force exerted by OHC

References

[Cohen et al. 1992] Y. E. Cohen, C. K. Bacon, and J. C. Saunders, "Middle ear development, III: Morphometric changes in the conducting apparatus of the Mongolian gerbil", *Hearing Res.* **62**:2 (1992), 187–193.

[Dannhof et al. 1991] B. J. Dannhof, B. Roth, and V. Bruns, "Length of hair cells as a measure of frequency representation in the mammalian inner ear", *Naturwissenschaften* **78**:12 (1991), 570–573.

[Edge et al. 1998] R. M. Edge, B. N. Evans, M. Pearce, R. C.-P., X. Hu, and P. S. Dallos, "Morphology of the unfixed cochlea", *Hearing Res.* **124**:1–2 (1998), 1–16.

[Geisler and Sang 1995] C. D. Geisler and C. Sang, "A cochlear model using feed-forward outer-hair-cell forces", *Hearing Res.* **86**:1–2 (1995), 132–146.

[Greenwood 1990] D. D. Greenwood, "A cochlear frequency-position function for several species: 29 years later", *J. Acoust. Soc. Am.* **87**:6 (1990), 2592–2605.

[Jimenez and Whitham 1976] J. Jimenez and G. B. Whitham, "An averaged Lagrangian method for dissipative wavetrains", *Proc. R. Soc. Lond. A* **349**:1658 (1976), 277–287.

[Karavitaki 2002] K. D. Karavitaki, *Measurements and models of electrically-evoked motion in the gerbil organ of Corti*, Ph.D. Thesis, MIT, 2002.

[Lim 1980] D. J. Lim, "Cochlear anatomy related to cochlear micromechanics: a review", *J. Acoust. Soc. Am.* **67**:5 (1980), 1686–1695.

[Lim and Steele 2002] K.-M. Lim and C. R. Steele, "A three-dimensional nonlinear active cochlear model analyzed by the WKB-numeric method", *Hearing Res.* **170**:1–2 (2002), 190–205.

[Loh 1983] C. H. Loh, "Multiple scale analysis of the spirally coiled cochlea", *J. Acoust. Soc. Am.* **74**:1 (1983), 95–103.

[Naidu and Mountain 2007] R. C. Naidu and D. C. Mountain, "Basilar membrane tension calculations for the gerbil cochlea", *J. Acoust. Soc. Am.* **121**:2 (2007), 994–1002.

[Parthasarathi et al. 2000] A. A. Parthasarathi, K. Grosh, and A. L. Nuttall, "Three-dimensional numerical modeling for global cochlear dynamics", *J. Acoust. Soc. Am.* **107**:1 (2000), 474–485.

[Rabbitt 2008] R. Rabbitt, "Efficiency of outer hair cell somatic electromotility", Poster session D9, Winter meeting (Phoenix, AZ) of the 31th Association for Research in Otolaryngology, 2008.

[Ren and Nuttall 2001] T. Ren and A. L. Nuttall, "Basilar membrane vibration in the basal turn of the sensitive gerbil cochlea", *Hearing Res.* **151**:1–2 (2001), 48–60.

[Smith 1968] C. A. Smith, "Ultrastructure of the organ of Corti", *Adv. Sci.* **24**:122 (1968), 419–433.

[Sokolich et al. 1976] W. G. Sokolich, R. P. Hamernik, J. J. Zwislocki, and R. A. Schmiedt, "Inferred response polarities of cochlear hair cells", *J. Acoust. Soc. Am.* **59**:4 (1976), 963–974.

[Steele and Puria 2005] C. R. Steele and S. Puria, "Force on inner hair cell cilia", *Int. J. Solids Struct.* **42** (2005), 5887–5904.

[Steele and Taber 1979] C. R. Steele and L. A. Taber, "Comparison of WKB calculations and experimental results for three-dimensional cochlear models", *J. Acoust. Soc. Am.* **65**:4 (1979), 1007–1018.

[Steele and Zais 1985] C. R. Steele and J. G. Zais, "Effect of coiling in a cochlear model", *J. Acoust. Soc. Am.* **77**:5 (1985), 1849–1852.

[Steele et al. 1993] C. R. Steele, G. Baker, J. Tolomeo, and D. Zetes, "Electro-mechanical models of the outer hair cell", pp. 207–215 in *Biophysics of hair cell sensory systems* (Paterswolde, 1993), edited by H. Duifhuis et al., World Scientific, Singapore, 1993.

[Steele et al. 1995] C. R. Steele, G. Baker, J. Tolomeo, and D. Zetes, "Cochlear mechanics", pp. 505–516 in *The biomedical engineering handbook*, edited by Z. D. Bronzino, CRC Press, Boca Raton, FL, 1995.

[Thorne et al. 1999] M. Thorne, A. N. Salt, J. E. DeMott, M. M. Henson, O. W. Henson, Jr., and S. L. Gewalt, "Cochlear fluid space dimensions for six species derived from reconstructions of three-dimensional magnetic resonance images", *Laryngoscope* **109**:10 (1999), 1661–1668.

[Yoon et al. 2007] Y.-J. Yoon, S. Puria, and C. R. Steele, "Intracochlear pressure and derived quantities from a three-dimensional model", *J. Acoust. Soc. Am.* **122**:2 (2007), 952–966.

Received 31 Jul 2008. Revised 16 May 2009. Accepted 17 May 2009.

YONGJIN YOON: yongjiny@stanford.edu
Stanford University, Mechanical Engineering, Durand Building, Room 262, Stanford, CA 94305, United States

SUNIL PURIA: puria@stanford.edu
Stanford University, Mechanical Engineering, Durand Building, Room 262, Stanford, CA 94305, United States

and

Stanford University, Otolaryngology — Head and Neck Surgery, Stanford, CA 94305, United States

CHARLES R. STEELE: chasst@stanford.edu
Stanford University, Mechanical Engineering, Durand Building, Room 262, Stanford, CA 94305, United States